ResearchGate

See discussions, stats, and author profiles for this publication at: https://www.researchgate.net/publication/364954578

A green and efficient technology to recover rare earth elements from weathering crusts

Article *in* Nature Sustainability · October 2022

DOI: 10.1038/s41893-022-00989-3

CITATIONS
13

READS
900

13 authors, including:

Runliang Zhu
Guangzhou Institute of Geochemistry, CAS
249 PUBLICATIONS **8,633** CITATIONS

SEE PROFILE

Xiaoliang Liang
Chinese Academy of Sciences
122 PUBLICATIONS **3,922** CITATIONS

SEE PROFILE

Shichang Kang
Chinese Academy of Sciences
17 PUBLICATIONS **1,164** CITATIONS

SEE PROFILE

Yuanyuan Wang
Chinese Academy of Sciences
6 PUBLICATIONS **66** CITATIONS

SEE PROFILE

Some of the authors of this publication are also working on these related projects:

Project nanomagnetite, catalysis, UV/Fenton View project

Project Synthesis, characterization, and properties of Keggin-Al30 pillared montmorillonite View project

All content following this page was uploaded by Yuanyuan Wang on 01 August 2023.

The user has requested enhancement of the downloaded file.

nature sustainability

Article

https://doi.org/10.1038/s41893-022-00989-3

A green and efficient technology to recover rare earth elements from weathering crusts

Received: 25 April 2022

Accepted: 27 September 2022

Check for updates

Gaofeng Wang[1,2,3], Jie Xu[1,2,3], Lingyu Ran[1,2,3], Runliang Zhu[1,2,3], Bowen Ling[4], Xiaoliang Liang[1,2,3], Shichang Kang[1,2,3], Yuanyuan Wang[1,2,3], Jingming Wei[1,2,3], Lingya Ma[1,2,3], Yanfeng Zhuang[5], Jianxi Zhu[1,2,3] and Hongping He[1,2,3]

Heavy rare earth elements (HREEs) such as Gd–Lu, Sc and Y are irreplaceable metals for a number of critical (including clean) technologies, but they are scarce. Ion-adsorption deposits, which form within weathering crusts, supply more than 95% of the global HREE demand. However, these deposits are currently mined via ammonium-salt-based leaching techniques that are responsible for severe environmental damage and show low recovery efficiency. As a result, the adoption of such techniques is restricted for REE mining, further exacerbating REE scarcity, which in turn could lead to supply chain disruptions. Here we report the design of an innovative REE mining technique, electrokinetic mining (EKM), which enables green, efficient and selective recovery of REEs from weathering crusts. Its feasibility is demonstrated via bench-scale, scaled-up and on-site field experiments. Compared with conventional techniques, EKM achieves ~2.6 times higher recovery efficiency, an ~80% decrease in leaching agent usage and a ~70% reduction in metallic impurities in the obtained REEs. As an additional benefit, the results point to an autonomous purification mechanism for REE enrichment, wherein the separation process is based on the mobility and reactivity diversity between REEs and metallic impurities. Overall, the evidence presented suggests that EKM is a viable mining technique, revealing new paths for the sustainable harvesting of natural resources.

Rare earth elements (REEs) are of vital importance to the world economy due to their widespread applications in various industries[1–3]. REEs can be categorized as light REEs (LREEs) and heavy REEs (HREEs), and HREEs have emerged as non-substitutable elements for many technologies, particularly for the new generation of sustainable energy applications, such as wind turbines, high-capacity energy storage and new energy vehicles[4–7]. As a result, the demand for HREEs continues to grow, which poses additional pressure on the REE mining industry. Ion-adsorption deposits (IADs), which are the dominant natural HREE repositories discovered in South China, contain more than 80% of the total HREEs and support 95% of the global demand[8,9]. However, as fundamental points in the HREE supply chain, local mining sites are experiencing enormous amounts of pressure due to the low recovery and severe environmental problems[9–12] associated with current mining techniques.

The adsorption of REE ions on clay minerals, predominantly on kaolinite and halloysite, has been suggested to be the main metallogenetic mechanism that forms IADs[13–15]. The adsorbed REEs can be recovered by a leaching process. To date, three major types of leaching techniques have been developed for IAD mining[16]—namely, pond leaching, heap leaching and in situ leaching, among which in situ leaching

[1]CAS Key Laboratory of Mineralogy and Metallogeny/Guangdong Provincial Key Laboratory of Mineral Physics and Material, Guangzhou Institute of Geochemistry, Chinese Academy of Sciences, Guangzhou, China. [2]CAS Center for Excellence in Deep Earth Science, Guangzhou, China. [3]University of Chinese Academy of Sciences, Beijing, China. [4]Institute of Mechanics, Chinese Academy of Sciences, Beijing, China. [5]School of Civil Engineering, Wuhan University, Wuhan, China. e-mail: hehp@gig.ac.cn

has become the dominant technique. During the leaching process, excessive amounts of leaching agents, commonly ammonium salts, are injected into the ore body to desorb REEs from the soil; subsequently, the leachate is collected for further REE extraction and purification. In a conventional in situ leaching practice, an ammonium salt solution is used not only as the ion exchanging agent but also to create the flow field that carries the REEs to the production well/pool. The large quantities of leaching agents used in conventional IAD mining practices have raised substantial environmental concerns, which include water contamination[3], soil degradation[17], forest destruction[9], landslides and large-scale waste generation[18]. For example, the acquisition of 1 t of rare earth oxide (REO) leads to the destruction of 200 m^2 of vegetation, the excavation of 300 m^3 of topsoil and the production of 2,000 t of tailings when the conventional pond leaching or heap leaching technique is applied[18]. It has been reported that in Ganzhou (one major mining region in China) alone, excessive mining has led to 302 abandoned mines, 191 Mt of tailings and 153 km^2 of destroyed forest[9]. Although in situ leaching lessens the necessity for topsoil excavation compared with pond leaching or heap leaching, it still consumes 7–10 t of ammonium salts to produce 1 t of REO[18] and introduces 0.2 t of ammonium into water and 1.9 t of ammonium into soils[17]. Repairing the damaged environments is predicted to cost 9% (~US$4.11 trillion) of China's national gross domestic product, according to a report from the World Bank[19]. Thus, ammonium-salt-based mining techniques have been restricted to protect the environment, which exacerbates the imbalance between HREE supply and demand. In addition, the current leaching techniques suffer from a lack of selectivity, and the extensive use of ammonium salts leads to coleaching of various metallic impurities (for example, Al^{3+}, Ca^{2+}, K^+ and Fe^{3+}) with REEs[20,21]. The high contents of impurities introduce further costs, both economic and environmental, for separation and purification[22,23]. Therefore, there exists an urgent need for developing environmentally and economically sustainable REE mining techniques.

Electrokinetic technology involves the application of a direct or alternating electric field to accelerate the migration of metals, organics and/or water[24,25]. This technique has been utilized in various scenarios, such as environmental remediation[26,27], soil dewatering/consolidation[28,29] and metal dissolution in low-permeability ores[30,31]. The advantage is twofold: the electrokinetic process accelerates the directional migration of ions[32,33] and simultaneously reduces the quantity of chemical agents required to transport ions[34]. Inspired by previous applications, we propose an innovative electrokinetic-mining (EKM) technique (Fig. 1a) for efficient and sustainable REE recovery. The newly developed EKM is projected to have the following characteristics: (1) the migration of REEs is enhanced by the applied electric field relative to conventional leaching techniques, where ion migration is governed by slow physical processes such as gravity, flow and/or concentration gradients; (2) the addition of leaching agents is substantially reduced since REEs are transported predominantly by the applied voltage gradient rather than by the flow of leaching agents; and (3) due to the use of lower amounts of leaching agents, the coleaching of metallic impurities from IADs is reduced. On the basis of the above considerations, we believe that the application of EKM for REE mining has the potential to promote REE recovery efficiency, lower leaching agent usage and enhance the purity of collected REEs. To the best of our knowledge, no experimental trials have been reported in which electrochemistry has been applied for REE mining.

In this study, we experiment with the newly developed EKM technique at three scales: bench-scale, scaled-up and on-site trials. Our experimental results from the different scales systematically confirm that high efficiency is achieved by the electromigration and electroosmotic mechanisms during EKM application. Furthermore, the synergy between these mechanisms results in a significant reduction in leaching agent usage and a substantial improvement in REE recovery efficiency compared with conventional leaching techniques. Specifically, our successful demonstration of EKM use in an actual IAD (14 t scale) in Guangzhou, South China, suggests its feasibility and potential to be extended to industrial-scale applications. More importantly, we observe an autonomous impurity purification (AIP) process occurring during EKM experiments: the metallic impurities (such as Al^{3+}, Fe^{3+} and Ca^{2+}) form secondary minerals, while the REEs migrate predominantly by electromigration and electroosmotic flow (EOF) (Fig. 1b,c). The AIP process significantly improves the purity of the collected REEs and promotes EKM as a next-generation REE mining technique. This research offers a potentially sustainable approach for recovering REEs and is expected to inspire more efforts to improve the EKM technique for recovering other critical Earth resources[35,36].

Results

Multiple phenomena take place during the EKM process—for example, electromigration, which promotes directional ion movement, and electroosmosis, which accelerates fluid movement via dissolved ions—and these mechanisms are closely related. To illustrate the efficiency of EKM and delineate the primary mechanisms, we systematically performed experiments at three scales.

Bench-scale EKM and conventional leaching

To evaluate the feasibility of EKM for REE recovery, bench-scale experiments were carried out in a homemade prototype (Fig. 2a,b) with a simulated IAD (see Supplementary Figs. 1–4 and Supplementary Table 1 for the details of the simulated IAD). The application of EKM with a small amount of added electrolyte can significantly enhance recovery efficiency (the ratio between the extracted REEs and the initial REEs contained in the soil; see equation (3) for the details), and the cumulative amount of the extracted REEs in the leachates (referred to as leachate REEs) for the 0M-EKM, 0.05M-EKM, 0.1M-EKM and 0.2M-EKM systems were 3.21, 35.14, 201.23 and 178.89 mg kg^{-1}, respectively (Fig. 2c). Note that there was a slight decrease in the extracted amount of leachate REEs when the electrolyte concentration increased from 0.1 to 0.2 M. This is attributed to the precipitation of REEs on the cathode plate (denoted as cathode REEs) during the EKM treatment, and the precipitates consist of REE hydroxides as confirmed by the characterization results (see Supplementary Fig. 5 and Supplementary Text 1 for the detailed analyses). During EKM, the current density increased with increasing electrolyte concentrations, and larger amounts of REE hydroxides were obtained using higher electrolyte concentrations (Supplementary Fig. 6), resulting in decreasing amounts of leachate REEs in the 0.2M-EKM system.

To compare the recovery efficiencies achieved with the EKM and conventional techniques, an ammonium leaching experiment using 0.1 M $(NH_4)_2SO_4$ was carried out (denoted as 0.1M-leaching), and the collected leachate REEs via both techniques were calculated (Fig. 2d). Notably, for the same treatment time required for EKM to reach equilibrium (the state at which the cumulative amount of the extracted REEs remained steady), the leachate REEs collected by the EKM method were ~4.6 times higher than those collected by the ammonium leaching technique (201 versus 44 mg kg^{-1}). In addition, the cathode REEs could be fully reclaimed by a posttreatment process (for example, acid washing). The final REE recovery efficiency (containing both the leachate and the cathode REEs) of the 0.1M-EKM system was thus calculated to be 84% (that is, ~315 mg kg^{-1}), which was 2.6 times higher than that achieved by the ammonium leaching technique (Fig. 2e). Moreover, EKM reached an equilibrium state more rapidly than the conventional leaching technique did (see Fig. 2d, Supplementary Fig. 7 and Supplementary Text 2); for example, the 0.1M-EKM experiment reached equilibrium within 270 min, while the 0.1M-leaching experiment was still far from equilibrium even after 878 min (Fig. 2d).

When an external electric field is applied, both ion motion and fluid flow are enhanced by electromigration and electroosmosis, which leads to a higher recovery rate. However, conducting a true comparison of the two techniques is not trivial since various factors affect the efficiency of both techniques.

https://doi.org/10.1038/s41893-022-00989-3

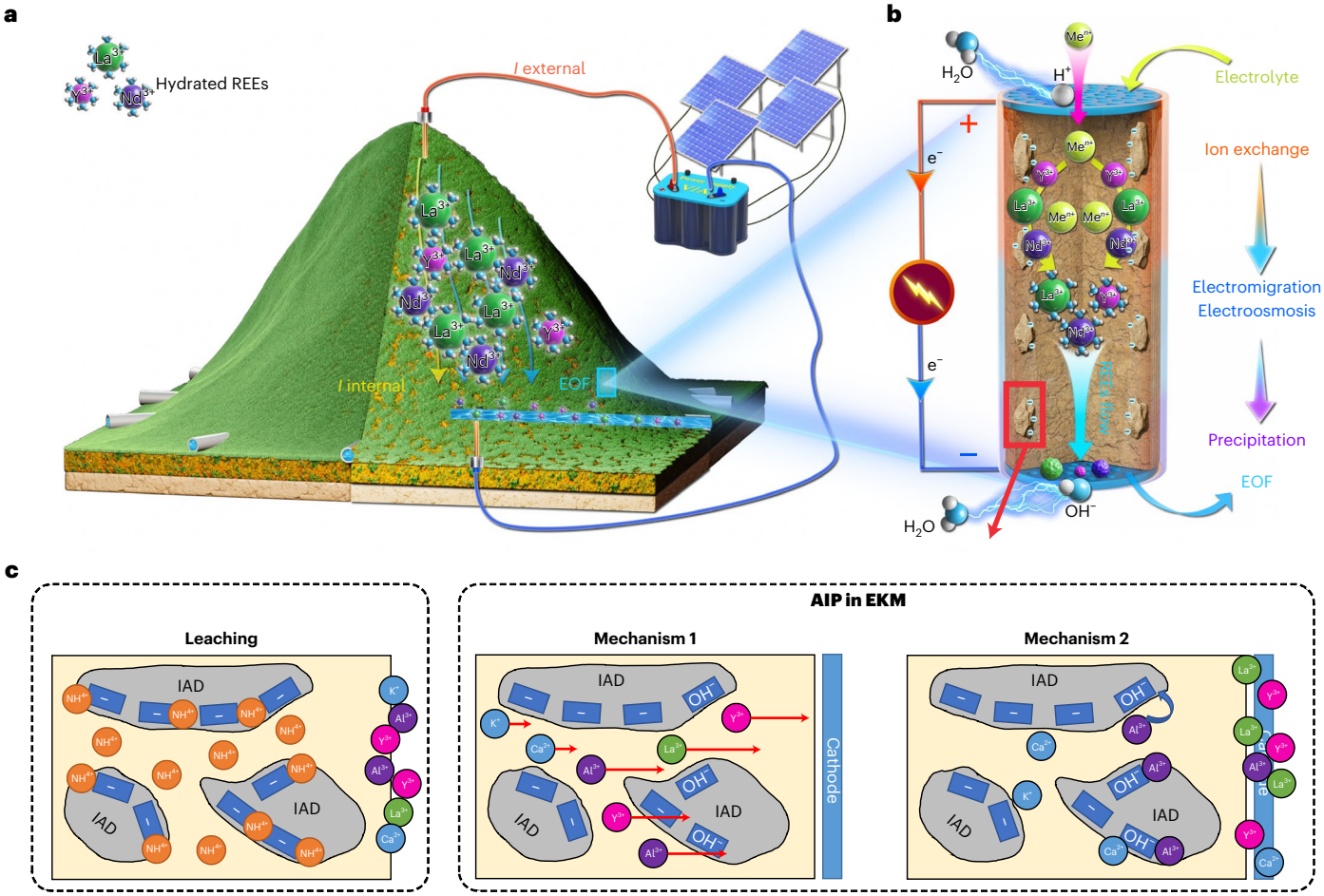

Fig. 1 | Illustration of IAD mining via EKM and AIP mechanisms. **a**, 3D illustration of in situ EKM for an IAD. The hydrated REEs are expected to be mobilized and extracted from an IAD under electrokinetic effects. *I*, current. **b**, Illustration of the EKM mechanisms for REE recovery, including ion exchange, electromigration, electroosmosis and the collection of EOF and precipitation. **c**, Comparison between conventional leaching and the EKM technique and schematic of the AIP process.

AIP mechanism

The extracted amounts of metallic impurities (Al^{3+}, Fe^{3+}, Ca^{2+}, K^{+}, Na^{+} and Mn (IV, VI and/or VII) species) in the leachates (Fig. 2f and Supplementary Table 2) using the EKM technique (15.83–94.44 mg kg^{-1}) were significantly lower than those obtained by using the conventional technique (260.77 mg kg^{-1}). This suggests that in addition to electromigration and EOF that drive cations unidirectionally, AIP occurs and substantially lowers the impurity content of the collected fluid. Specifically, the EKM technique leads to a 66% decrease in metallic impurities in the collected contents (Fig. 2f) compared with those using the conventional technique.

We further investigated AIP by analysing the contents of each impurity. As the electrolyte concentration was increased from 0.05 to 0.2 M, the total amount of low-valent impurities (for example, Ca^{2+}, K^{+} and Na^{+}) remained the same and even decreased, while the collected REEs increased dramatically (Fig. 2c,f). This suggests that low-valent ions move towards the cathode more slowly. We infer that such a result can be explained by the mobility differences caused by the external electric field. During EKM, the main driving force for the transport of REEs and metallic impurities is the electric field force—that is, electromigration and electroosmotic effects. The subjected electric field force for a specific ion is correlated with its ionic valance[24,33,37], wherein high-valent ions experience a larger electric field force than low-valent ions experience in the same system. Consequently, high-valent ions (for example, REEs) arrive at the cathode more quickly than low-valent metallic impurities (for example, Ca^{2+} and K^{+}), which forms a high potential barrier and impedes the transport of low-valent metallic impurities towards the cathode. We therefore conclude that the first mechanism of AIP involves the mobility diversity.

For the high-valent ions, primarily Al^{3+}, we noticed that a high content of Al species precipitated on the cathode plate after EKM treatment, as detected by energy-dispersive X-ray spectroscopy (Fig. 3a). The X-ray photoelectron spectroscopy (XPS) analyses of the Al 2*p* (Fig. 3b), Al 2*s* (Fig. 3c) and O 1*s* (Fig. 3e) spectra indicated that the precipitates were mainly composed of $Al(OH)_3$ and meta-aluminates (see Supplementary Text 3 for a detailed analysis). During conventional leaching, water-soluble and exchangeable Al is the dominant source of Al impurities, wherein Al exists in the forms of $Al^{3+}{\cdot}nH_2O$ or $[Al(OH)_m]^{3-m}{\cdot}nH_2O$[38,39]. These Al species can be readily leached out and coexist with REEs in the leachates. However, during the EKM process, an alkaline pH environment (pH = 10.5–11.5, as shown in Supplementary Fig. 8) is generated around the cathode due to the electrolysis of water, resulting in the formation of $Al(OH)_3$ (when pH > 4.4) and AlO_2^- (when pH > 8.5)[39]. The $Al(OH)_3$ precipitates are retained on the cathode plate, while the negatively charged AlO_2^- ions are transported towards the anode (that is, opposite to the direction of migration of REEs during EKM), resulting in separation between REEs and Al^{3+} impurities.

Similarly, impurities of Fe^{3+} and Mn (IV, VI and/or VII) can also be inhibited by generating precipitates of the metal hydroxides (for example, $Fe(OH)_3$ and $Mn(OH)_2$) and negatively charged compounds

https://doi.org/10.1038/s41893-022-00989-3

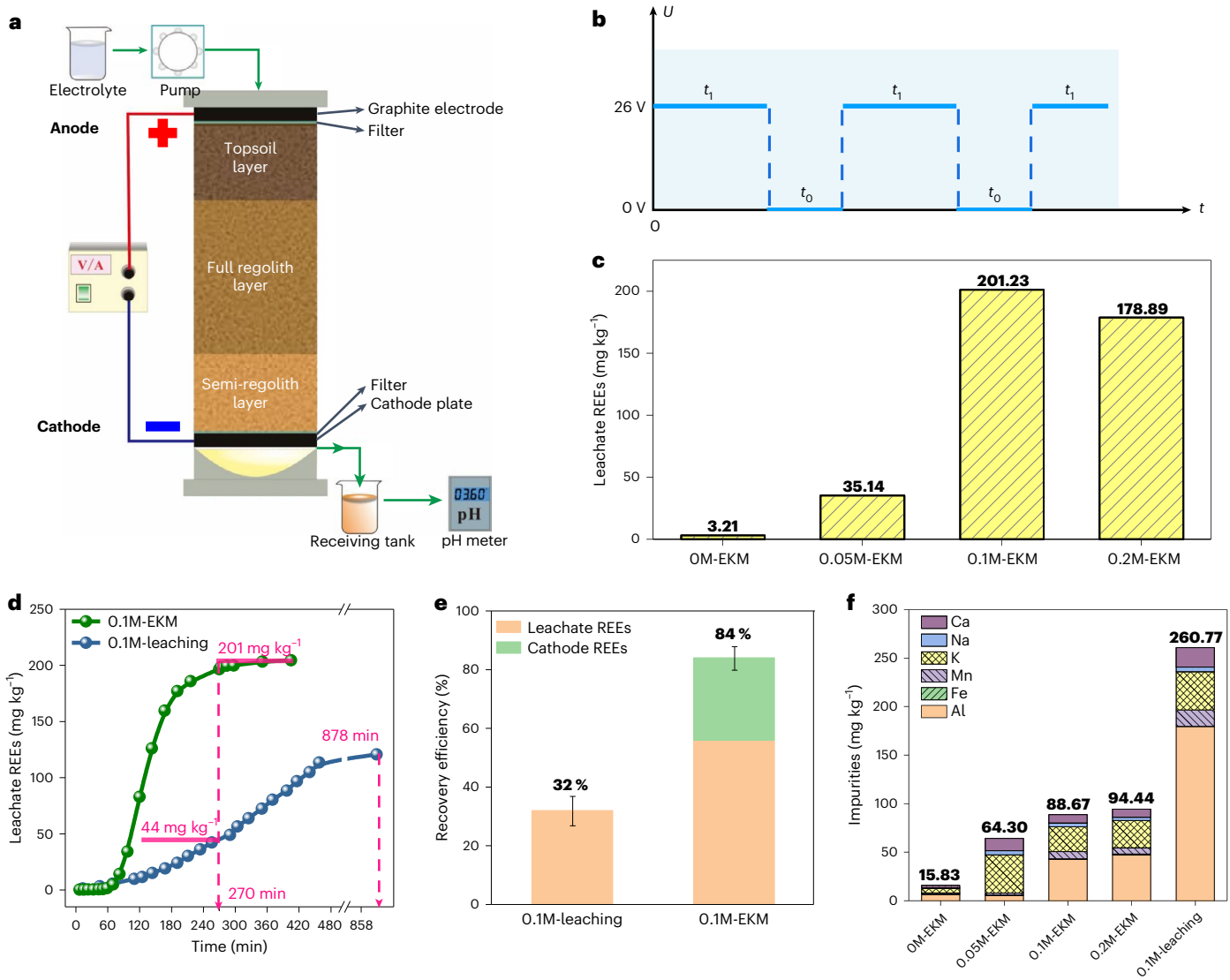

Fig. 2 | Setup for the bench-scale EKM experiments and the obtained results. a, The experimental setup for the bench-scale EKM experiments. **b**, The intermittent voltage (U) applied during the bench-scale EKM experiments, where t_1 and t_0 represent the duration of power on and power off, respectively. **c**, Effect of the electrolyte concentration on the cumulative amount of extracted REEs in the leachates. **d**,**e**, Comparison of the cumulative amounts of extracted REEs in the leachates (**d**) and the REE recovery efficiency achieved by using EKM and the conventional techniques (**e**). **f**, Comparison of the cumulative amounts of the extracted impurities in leachates achieved by using EKM and the conventional techniques. The error bars represent the mean ± standard deviation. All EKM experiments were conducted at a 0.5 V cm^{-1} voltage gradient.

(for example, FeO_2^- and MnO_4^{2-}) (Supplementary Reactions 1–3). As the amounts of both iron and manganese impurities were very low in the system (for example, 0.28 and 7.43 mg kg^{-1}, respectively), we did not detect their precipitates on the cathode plate or in the nearby soils.

The decrease in Ca^{2+}, the second-most-abundant metallic impurity, can be attributed to the formation of $CaCO_3$ near the cathode (as detected by the Ca 2p XPS spectrum) (see Fig. 3d and Supplementary Text 3 for a detailed analysis). The second mechanism of AIP is thus induced by the reactivity diversity between REE and other active metal ions. Overall, the selective recovery of REEs achieved using the EKM technique by the AIP mechanism is beneficial for the further purification and separation of REEs.

Scalability investigations for EKM

To assess the scalability of the EKM technique, scaled-up experiments were carried out at the kilogram scale (20 kg) in a larger EKM setup (Supplementary Fig. 9) with a similar weathering crust sample (see Supplementary Table 3 and Supplementary Fig. 10 for the details). In the scaled-up experiments, we found that the current density was dramatically higher than that in the bench-scale experiments at the same voltage gradient (Supplementary Fig. 11), which was attributed to a lower total effective electric resistance in the scaled-up experiments (16ρ; see Supplementary Text 4 for the calculation method) than in the bench-scale experiments (66ρ). This finding suggests that the applied voltage and the electrolyte dosage can be reduced in larger-scale applications.

The collected volume of leachate exhibited an approximately linear increase with treatment time in both EKM and the conventional leaching experiments (Fig. 4b). We calculated the EOF flux of the EKM technique (10.00×10^{-4} kg m^{-2} s^{-1} at a voltage gradient of 0.07 V cm^{-1}), which was significantly higher than the diffusive flux of the conventional leaching technique (3.54×10^{-4} kg m^{-2} s^{-1} without an applied voltage gradient). This result demonstrates that the applied electric field can markedly accelerate the migration of hydrated REEs. Similar to the bench-scale experiments, the REE concentrations in the leachates displayed a mountain-type pattern with increasing treatment

https://doi.org/10.1038/s41893-022-00989-3

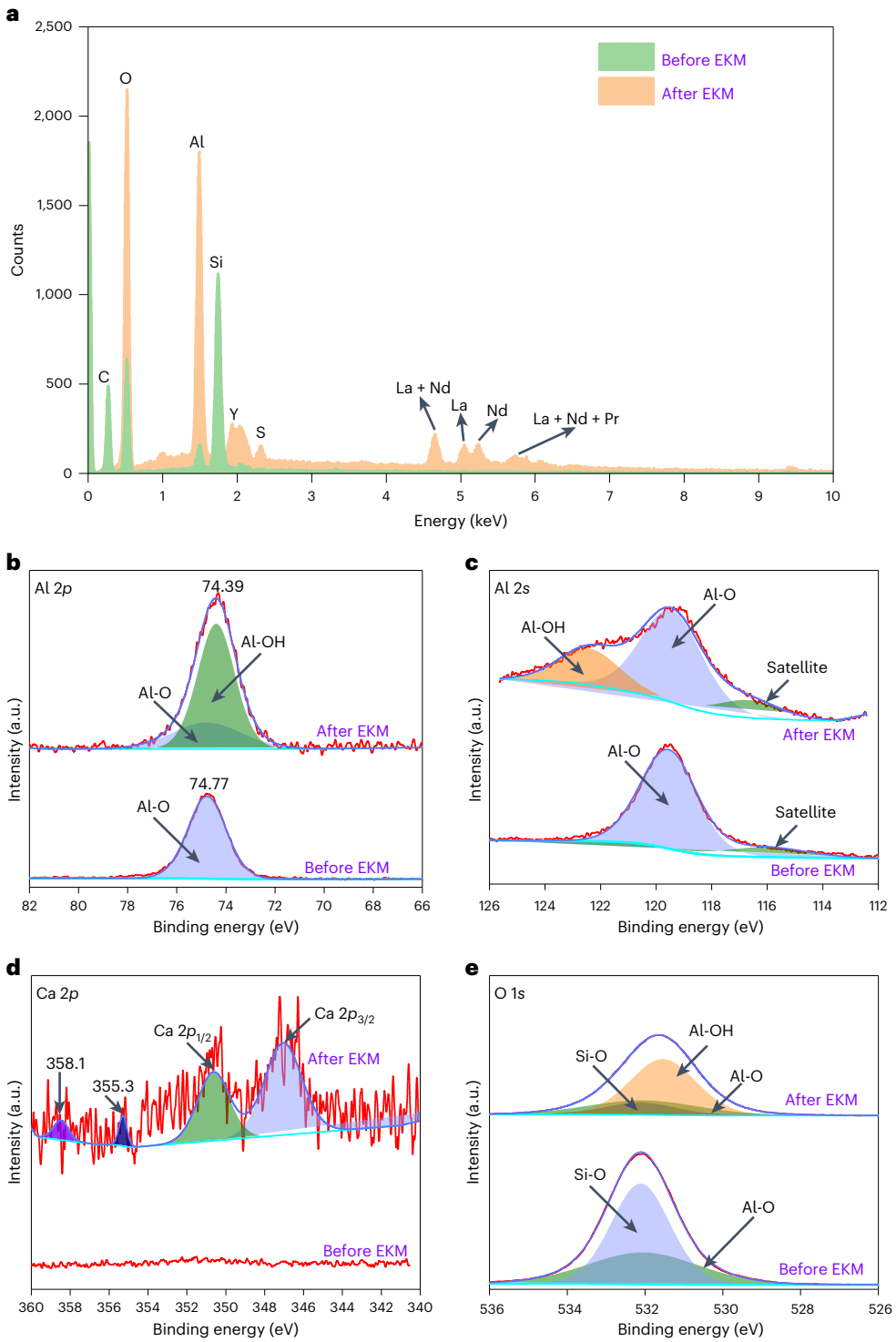

Fig. 3 | Analysis of precipitates on the cathode plate after EKM treatment. a, Energy-dispersive X-ray spectroscopy results from the substances on the cathode before and after EKM treatment. **b**–**e**, High-resolution XPS results for Al 2*p* (**b**), Al 2*s* (**c**), Ca 2*p* (**d**) and O 1*s* (**e**) of the substances on the cathode before and after EKM treatment.

time. Note that the maximum was reached at approximately 23 h in the EKM experiment and 105 h in the conventional leaching experiment (Supplementary Fig. 12). This further verified that the migration of REEs during EKM was much faster than that during conventional leaching. Consequently, the scaled-up experiments achieved a recovery efficiency of 96% within 67 h by using the EKM technique, while that using the conventional technique was only ~62% at 130 h (Fig. 4c). This suggests that the EKM technique can achieve a higher recovery efficiency and requires less treatment time, consistent with the findings in our bench-scale experiments.

Notably, in the case of the EKM technique, the content of metallic impurities (130.06 mg kg^{-1} in total) in the collected leachate was far lower than that of REEs (~2,000 mg kg^{-1}) (Fig. 4d); also, it was much lower than the content of metallic impurities (332.58 mg kg^{-1}

https://doi.org/10.1038/s41893-022-00989-3

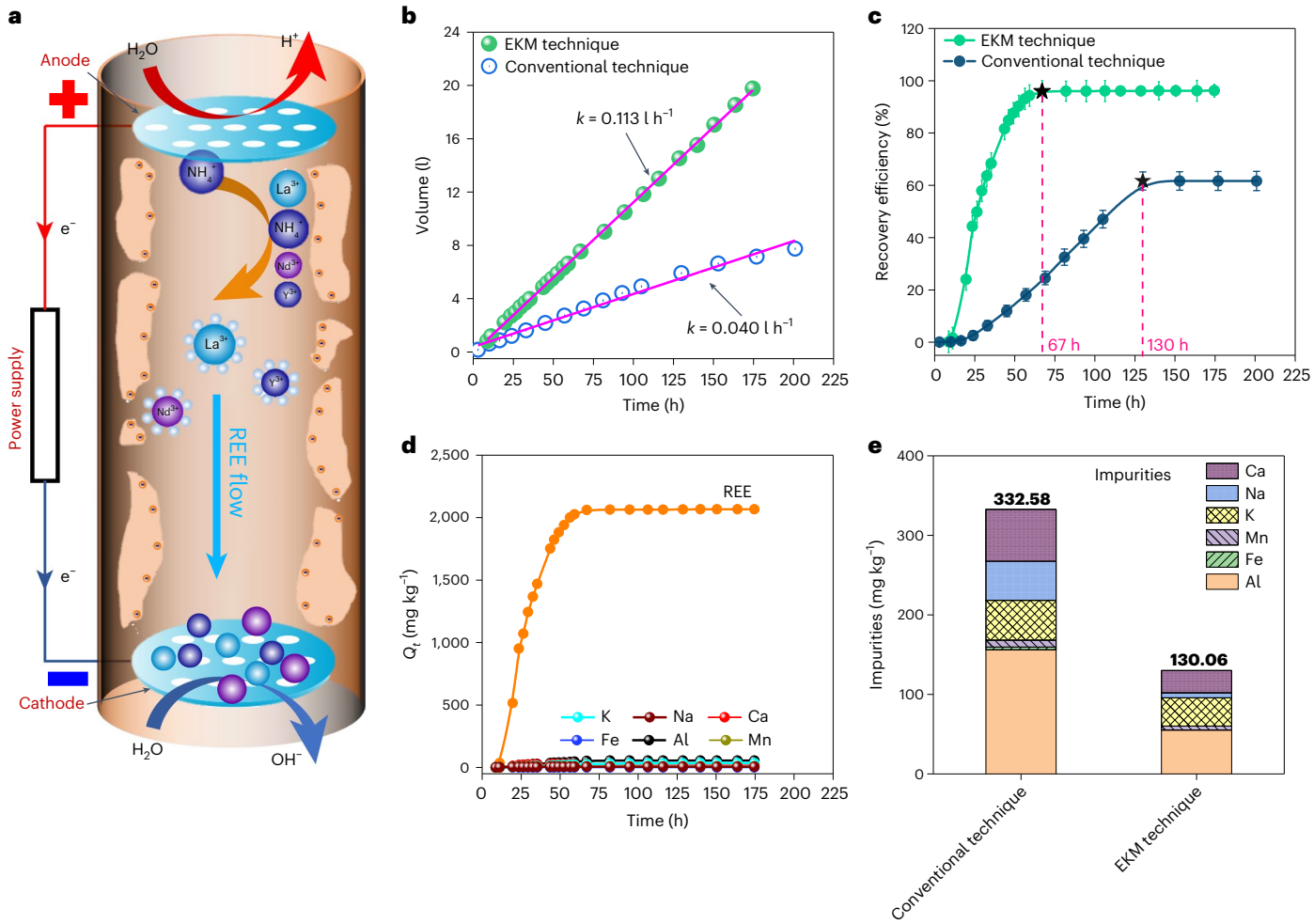

Fig. 4 | Setup for the scaled-up EKM experiments and the obtained results. a, The experimental setup for the scaled-up experiments. **b**,**c**, Comparison of the collected volume of the leachate (**b**) and the recovery efficiencies achieved by using EKM and the conventional technique (**c**). **d**, Comparison of the cumulative amount between the extracted REEs and metallic impurities by using the EKM technique. **e**, Comparison of the cumulative amount of the extracted metallic impurities by using EKM and the conventional technique. The error bars represent the mean ± standard deviation. All EKM experiments were conducted at a 0.07 V cm^{-1} voltage gradient.

in total) using the conventional technique, showing a reduction of 61% (Fig. 4e and Supplementary Table 4). This result suggests that AIP occurred at different scales and exhibited good scalability. We thus found that EKM exhibits greater selectivity for REEs than ammonium leaching techniques.

Application of EKM to an actual IAD

On the basis of the successful bench-scale and scaled-up experiments, we applied the EKM technique to an actual IAD (~14 t scale) via an on-site field experiment. The basic properties of the IAD, including the dimensions (Supplementary Fig. 13a,b), the water content (Supplementary Fig. 13c–e), the concentration of ion-exchangeable REEs (Supplementary Fig. 14) and mineral components (Supplementary Fig. 15), were obtained on the basis of the detected values from 24 sampling points (Supplementary Tables 5 and 6).

The experimental setup for field EKM is shown in Fig. 5a, and two mining sections were achieved by three rows of electrodes. Before EKM treatment, the experimental ore was prewetted with electrolyte ($(NH_4)_2SO_4$) solution until the effective electrical resistance of the experimental ore reached its lowest value and remained constant (Supplementary Fig. 16). A voltage gradient of 0.3 V cm^{-1} (Fig. 5b) was applied for the field EKM treatment on the basis of previous work[40].

During the first stage (0–132 h), the current decreased from 1.67 to 0.50 A (Fig. 5c), suggesting that the conductive ions (primarily REEs) migrated out of Section 1. By detecting the REE concentration in the ore, we found that the REEs were transported from the anodes to the cathodes (Fig. 5e).

During the second stage (132–264 h), an intermittent voltage gradient of 0.3 V cm^{-1} was applied with cycles of 20 min for power on and 10 min for power off. Previous work[41–43] has suggested that using an appropriate intermittent power output can lower energy consumption and enhance the acidification process, which improves removal efficiency by mobilizing metals. The protocol adopted in our experiment (the power-on time was twice the power-off time) achieved the highest removal efficiency and the lowest energy consumption, as demonstrated by heavy metal (for example, Cu, Cd and As) removal experiments[42]. In this stage, the current decreased gradually from ~0.9 to ~0.2 A (Fig. 5d), which reflected the migration of REEs out of Section 2 as well. The REE concentration heatmap (Fig. 5e) demonstrates that the REEs were transported from the anodes to the cathodes. As the experimental ore was not separated from the surroundings, a part of the EOF could not be collected during this field experiment. Nevertheless, such engineering problems can be readily addressed during practical applications by controlling the location of the collecting reservoir. The

https://doi.org/10.1038/s41893-022-00989-3

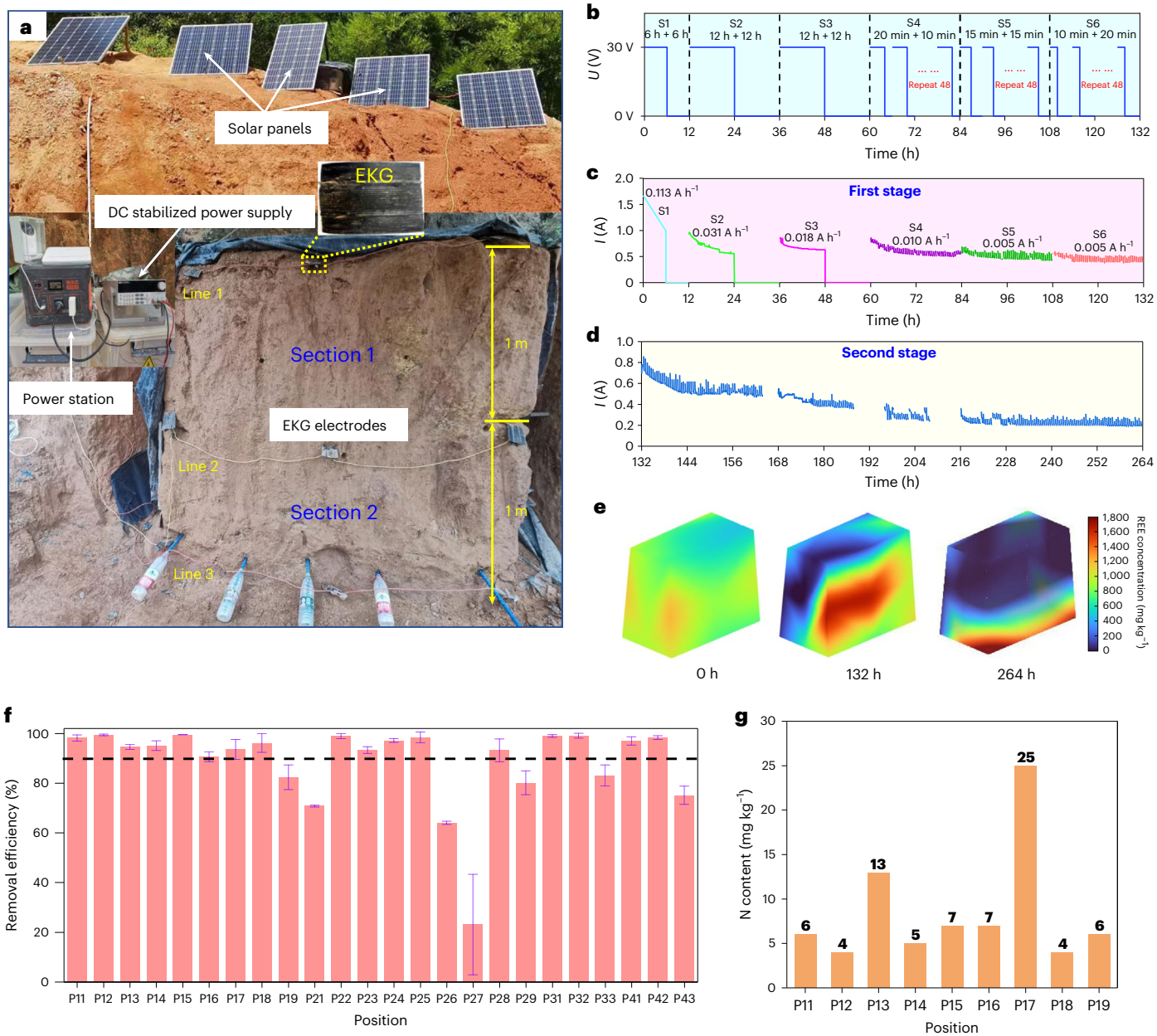

Fig. 5 | Setup for the on-site field EKM experiment and the obtained results. **a**, The experimental setup for the on-site field EKM experiment. **b**, Continuous and intermittent voltages applied during the first stage of the field EKM experiment. **c**,**d**, The variation in the electric current in the first (**c**) and second (**d**) stages of the EKM treatment. **e**, 3D heatmaps showing the variation in ion-exchangeable REE concentrations during EKM. **f**, Removal efficiencies of REEs in 24 representative positions. The error bars represent the mean ± standard deviation. **g**, The residual N content in the soil after the field EKM treatment. All EKM experiments were conducted at a 0.3 V cm^{-1} voltage gradient.

mining efficiency of the field EKM experiment was therefore evaluated by calculating the removal efficiency (see equation (4) for the calculation method) of REEs from the ore. We calculated the recovery efficiencies of 24 representative positions (Supplementary Fig. 13c), most of which were higher than 90% (Fig. 5f).

To evaluate the possible environmental impacts of the field experiment associated with ammonium salts, we measured the residual water-soluble nitrogen (N) content in the soil after field EKM. Notably, the residual water-soluble N contents of most of the sampling sites were lower than 10 mg kg^{-1} (Fig. 5g). This value was significantly lower than that in mining tailings (49.5–126.0 mg kg^{-1}) produced from the use of conventional leaching techniques even after the tailings are abandoned for many years[44].

Discussion

Mechanisms underlying the high REE recovery efficiency

As shown in the previous section, our experimental results demonstrate that EKM is an efficient and scalable technique that shows high REE recovery efficiency for IAD mining. The underlying mechanisms were demonstrated to involve electromigration, electroosmosis and directional control of REE migration. The detailed discussion is provided in the Supplementary Information.

Techno-economic analysis of EKM

To assess the economic feasibility of EKM, comparative techno-economic analysis of EKM and conventional REE mining techniques was conducted (see the Supplementary Information and

Supplementary Tables 7 and 8 for the detailed procedures and calculations). Comparative techno-economic analysis was performed to assess the annual production of 2,000 t of REO by using the conventional and EKM techniques. Supplementary Table 9 shows the cost breakdown for the two techniques. The total cost of producing 2,000 t of REO per year is US$52,056,727 using the conventional technique and US$18,558,602 using the proposed EKM technique. Notably, the annual cost for conventional leaching is 2.8 times higher than that for EKM, demonstrating the economic feasibility of the EKM technique. The major cost drivers for conventional leaching are the indirect cost of postmining environmental remediation (constituting 63.30% of the total cost) and the resource tax (constituting 28.68% of the total cost) (Supplementary Fig. 19), while the major cost drivers for the EKM process are the resource tax (constituting 80.45% of the total cost) and total capital investment (constituting 15.81% of the total cost). This is because the EKM technique requires higher capital investment for equipment purchasing and installation than the conventional technique. To provide an example, the production costs for obtaining 1 t of REO by the conventional and the EKM techniques are US$26,019 and US$9,279 (Supplementary Table 10), respectively. Moreover, the environmental compatibility of the mining infrastructure and the sustainability of the mining process require full analysis of the entire production chain—for example, by life cycle assessment. Life cycle assessment will be needed in the future not only to robustly confirm the sustainability of the EKM technique but also to facilitate decision-making in industrial applications.

Towards sustainable REE mining via EKM

On the basis of the above results, the proposed EKM technique may serve as a next-generation technique for sustainable REE mining due to its low environmental impact, high REE recovery efficiency and selectivity, and low economic cost. The dramatic decrease in the usage of ammonium salts during EKM is key to its low environmental impact during REE mining. The current REE mining techniques have substantial environmental impacts, primarily resulting from the excessive usage of leaching agents (predominantly ammonium salts)[45–47]. Conventional techniques generally consume 7–10 t of $(NH_4)_2SO_4$ to produce 1 t of REO[18], causing severe ammonium contamination. In the EKM system, only a small amount of electrolyte is used to desorb REEs and increase the conductivity of the system (Supplementary Figs. 6 and 16). Notably, the use of $(NH_4)_2SO_4$ was reduced by ~73% and ~80% in the scaled-up and field EKM experiments, respectively, compared with that in the conventional technique. The sharp decrease in the usage of ammonium salts in the EKM technique can significantly decrease their associated environmental risks. For example, the residual N content at most soil sampling sites after on-site field EKM was lower than 10 mg kg^{-1} (Fig. 5g), which is benign to the environment, and thus environmental contamination by ammonium was prevented.

Additionally, the power consumption (see equation (5) for the calculation method in the Methods) was calculated to be only 1.96 kWh in the field EKM experiment (Supplementary Fig. 20)—that is, it takes 0.32 kWh to mine 1 m^3 of the IAD. This energy cost is far lower than that of the current applications of electrokinetic technology, such as in soil remediation[48,49] (tens of kWh m^{-3}) and electrokinetic dewatering[50] (~6 kWh m^{-3}). The energy consumption is slightly higher than for conventional mining techniques, but the associated environmental impact of such low electricity usage during EKM is negligible. Furthermore, the electricity is supplied by solar panels, which are clean, economical and convenient to obtain.

The significantly enhanced REE recovery efficiency (>90%) of the EKM technique can help maintain the vulnerable HREE supply chain and reduce environmental impacts. More than 95% of the global HREEs are mined from IADs in South China[8,9], but conventional mining techniques have low recovery efficiency (40–60%)[9,17], leaving a considerable amount of REEs in IAD tailings after mining. This not only is a huge waste of valuable REEs, especially HREE resources, but also results in potential risks to the local environment since REEs are unstable after being activated with electrolytes. Recycling these low-grade REEs from IAD tailings by secondary mining is a possible solution, but this requires high economic and environmental costs[7]. The exceptionally high recovery efficiency of the EKM technique is predicted to obtain more REEs from a mining site, which would help alleviate the intense demand for REEs, especially for scarcer HREEs. Moreover, the high recovery efficiency of EKM results in lower amounts of REE residues in soils, which is beneficial to the local environment.

The EKM technique can tremendously lower the amounts of metallic impurities in the collected REEs, lowering costs for additional separation and purification. The current leaching techniques lack selectivity; REEs and metallic impurities are therefore coleached[20]. Similar to REEs, these metallic impurities (for example, Al^{3+} and Fe^{3+}) can precipitate with precipitation agents (that is, oxalic acid or ammonium bicarbonate) during the hydrometallurgy process, resulting in a significant reduction in the purity of the final REO product[22,23,51]. These metallic impurities therefore need to be separated from REEs. Various methods have been proposed to remove metallic impurities[20,23,39], such as neutralizing hydrolysis with acid and alkali, solvent extraction with saponifying naphthenic acid, and complexation with complexing agents. Clearly, treatment for these metallic impurities requires the use of additional chemical agents, which increases the economic cost and introduces environmental hazards. Due to the AIP process, the EKM technique exhibits a transformative feature—namely, REE selectivity—compared with conventional processes (Fig. 1c). The selective recovery of REEs improves the purity of REEs, which reduces costs for further separation and purification.

In summary, EKM is a sustainable technique, both environmentally and economically, that enables green, efficient and selective recovery of REEs from weathering crusts, and its feasibility is demonstrated at both the laboratory and field scales. We successfully applied this EKM technique to an actual IAD (14 t scale) and achieved a recovery efficiency higher than 90%, which sets a paradigm of the EKM technique for practical applications. Moreover, we demonstrated an AIP mechanism involved in the EKM technique, which significantly increases the purity of the collected REEs when compared with conventional techniques. Our results strongly support the green and efficient EKM process as a new generation of mining technique for REE recovery. It can contribute to sustainable REE production and help maintain the vulnerable HREE supply chain. In addition, the EKM technique serves as a possible solution for sustainably recovering other critical metals under conditions in which the metals exist in ionic and/or movable states, such as carbonate clay-type lithium, laterite nickel and weathered crust elution-deposited scandium ores.

Methods

Samples and sampling sites

The samples used in the bench-scale and scaled-up experiments were collected from a weathering crust in Guangzhou, South China (Supplementary Fig. 1). The collected samples were dried at room temperature and meshed to pass through a 0.9 mm mesh before being used.

Bench-scale EKM experiments

The bench-scale EKM experiments were carried out using a prototype setup containing a cylindrical soil column, two electrodes and a DC power supply (5A32 V, Lodestar). Initially, 110 g of the topsoil layer, 220 g of the full regolith layer and 110 g of the semi-regolith layer samples were placed in the soil column and compressed to a height of 13 cm with a diameter of 6 cm, achieving a bulk density of 1.20 g cm^{-3} for the simulated weathering crust. Two electrodes were inserted on each side of the soil column to act as the anode and the cathode. Numerous 0.5 mm holes were drilled into the electrodes to allow for the flow of water. The electrodes and the soil samples were separated by filter papers to prevent soil particles from being washed out. Then, 150 ml

of electrolyte solution (0, 0.05, 0.1 or 0.2 M $(NH_4)_2SO_4$ (99.99 wt%, Aladdin)) at pH 5.31 was pumped into the soil column. This produced an initial water content of ~30% for the sample, and no leachate was acquired due to the water adsorption capacity of the simulated weathering crust. Subsequently, the system was subjected to an intermittent voltage (2 or 0 V cm^{-1}) for the EKM treatment. Deionized water was continuously introduced from the anode at a flow rate of 0.4 ml min^{-1} (18.2 Ω, MUL-9000) with a peristaltic pump (F01A, Kamoer) to keep the system wet. The leachate was collected and analysed by inductively coupled plasma–optical emission spectrometry (ICP–OES). The pH of the leachate was monitored with a pH meter (FE28-Standard, Mettler). For comparison, conventional leaching experiments without the application of voltage were carried out, and all other conditions were kept the same as those of the EKM experiments.

Scaled-up EKM experiments

The scaled-up experiments were performed in a larger EKM setup with a diameter of 20 cm and a height of 50 cm. The experimental procedures were similar to those of the bench-scale experiments. Compared with the bench-scale experiments, the sample weight was amplified approximately 50 times (20 kg versus 0.44 kg), and the bulk density of the soil sample was increased (1.39 g cm^{-3} versus 1.20 g cm^{-3}). The soil sample was prewetted using 6 l of electrolyte solution (0.05 M $(NH_4)_2SO_4$), and a total of 15 l of electrolyte solution was added during EKM; the rest was introduced at a flow rate of 2.5 ml min^{-1} with a peristaltic pump. After all the targeted electrolyte solutions were added, deionized water was continuously introduced from the anode at a flow rate of 2.5 ml min^{-1} to keep the system wet. After the system received the first drop of leachate, a voltage gradient of 0.07 V cm^{-1} was applied between the anode and the cathode for the EKM treatment. For comparison, conventional leaching experiments without the application of voltage were also carried out, and all other conditions were kept the same as those of the EKM experiments.

On-site field EKM experiment

The on-site field EKM experiment was carried out in an actual IAD at the site where the samples used for the bench-scale and scaled-up experiments were collected. We separated a cuboid area (~2 m × 1.5 m × 2 m) for the field EKM experiment (Supplementary Fig. 13a,b). According to the volume (~6.18 m^3) and soil density (~2.2 g cm^{-3}) of the selected area, the calculated weight was ~14 t. On the basis of the detected values from 24 sampling points (Supplementary Tables 5 and 6), the water content and concentration of ion-exchangeable REEs in the ore were described using 3D heatmaps (Supplementary Fig. 13c–e), and the calculated average values were 14% and 878 mg kg^{-1}, respectively (see Supplementary Text 5 for the detailed methods). From top to bottom, the ratios of ion-exchangeable LREE/HREE decreased from ~4 to ~1, indicating variations in the LREE and HREE contents of the ore (Supplementary Fig. 14 and Supplementary Table 5). The main mineral components in the IAD were kaolinite, halloysite and iron oxides (for example, hematite and goethite), and minor amounts of montmorillonite appeared in the lower sections of the ore (Supplementary Fig. 15).

The field EKM experiment included procedures for installing electrodes, prewetting and EKM. The ore body was initially drilled, producing several holes front to back for the installation of electrokinetic geosynthetic electrodes. Three pieces of electrokinetic geosynthetic electrodes (0.1 m × 1.1 m) were inserted into the holes at intervals of 1 m to act as the anodes or cathodes, and the electrodes were connected in parallel. Then, several 20-cm-deep holes were drilled into the top surface of the ore for the injection of electrolyte solution ($(NH_4)_2SO_4$). Before EKM treatment, the experimental ore was prewetted with 2,100 l of electrolyte solution to achieve a water content of ~30% in the soil; the experimental ore was wetted, but no leachate was collected due to the water retention capacity of the soil. The electrolyte concentration was determined to be 0.075 M on the basis of the added volume of water (2,100 l) and the dosage of electrolyte (~2 times the molar ratio of $(NH_4)_2SO_4$ to REEs, similar to that in the scaled-up experiments). Finally, a voltage gradient of 0.3 V cm^{-1} was applied between the anodes and cathodes for the EKM treatment to achieve an initial current of ~2.0 A, which is similar to the suggested optimal current (0.2–2 A)[40] for ion and water migration in soils. The electricity was generated using five 200 W solar panels (DJB200, Guanghe) that were connected in parallel, stored with four 1,260 Wh portable power stations (DELTA1300, ECOFLOW) and transformed from AC to DC using a DC stabilized power supply (IT6722, ITECH).

Analytical methods

The concentrations of REEs and metallic impurities were determined by ICP–OES, which was conducted on an Agilent 730 spectrometer. For leachates, 10 ml of the solution was acidified with 10 µl of ultrapure concentrated nitric acid (1% v/v) and then passed through a 0.22 µm filter membrane before measurement. For solid samples, 1 g of the solid sample was added into a centrifugal tube containing 10 ml of $(NH_4)_2SO_4$ (0.2 M, pH = 5.32). The tube was placed in a shaker for vigorous agitation for 24 h to allow for ion exchange between the REEs/metallic impurities and NH_4^+. The mixture was then centrifuged at 6,000 *g* for 10 min to obtain the supernatant. The subsequent procedures were the same as those for leachate measurement. Rh was used as an internal standard to calibrate the drift of the instrument, and several United States Geological Survey and Chinese rock and sediment standards (GSR-2, GSR-3, GSD-09, GSD-11, SARM-4, W-2 and AGV-2) were used for external quality control during the measurements. The analytical precision was better than 3% relative standard deviation. Since the EKM experiments were carried out at various scales, the extracted amounts of the REEs/metallic impurities were normalized to soil weight with a unit of mg kg^{-1} according to equation (1):

$$Q = \frac{C \times V}{m} \tag{1}$$

where C (mg l^{-1}) is the concentration of the REEs/metallic impurities in the leachates or exchanged from the solid, V (l) is the volume of leachates or the added $(NH_4)_2SO_4$, m (kg) is the soil weight and Q is the calculated amount of REEs/metallic impurities normalized to soil weight (mg kg^{-1}). The cumulative amount of the extracted REEs/metallic impurities in the collected leachates at time t (Q_t, mg kg^{-1}, normalized to soil weight) was calculated according to equation (2):

$$Q_t = \frac{\int_0^t C_t V_t \mathrm{d}_t}{m} \tag{2}$$

where C_t (mg l^{-1}) and V_t (L) are the REE concentration and collected volume of the leachate at time t, respectively, and t (min) is the EKM treatment time. The recovery efficiency using EKM or the conventional leaching technique was calculated according to equation (3):

$$\text{Recovery efficiency} = \frac{Q_{\text{total}}}{T_{\text{ion}}} \times 100\% \tag{3}$$

where Q_{total} (mg kg^{-1}) is the cumulative extracted amount of REEs in the leachate and reclaimed from the cathode after EKM treatment, and T_{ion} (mg kg^{-1}) represents the ion-exchangeable REE concentration before EKM treatment. In the field experiments, the removal efficiency of EKM for REEs was calculated according to equation (4):

$$\text{Removal efficiency} = \frac{C_{\text{ini}} - C_{\text{equi}}}{C_{\text{ini}}} \times 100\% \tag{4}$$

where C_{ini} and C_{equi} (mg kg^{-1}) represent the ion-exchangeable REE concentrations in the soil before and after EKM treatment. The pH of leachates and solid samples was measured by using a pH meter. In

the former case, the pH was measured directly; in the latter case, 2 g of solid sample was first dispersed into 5 ml of degassed deionized water and then left to settle for 2.5 h before measurement. The energy consumption during the field EKM experiment was calculated according to equation (5):

$$\text{Energy consumpton} = \int_0^t U_t I_t \mathrm{d}t \quad (5)$$

where U_t (V) is the applied voltage and I_t is the corresponding current at EKM treatment time t.

Uncertainty analysis

In this work, uncertainty originated mainly from two routes: experiments (type A uncertainty) and measurements (type B uncertainty). For accuracy, each experiment was repeated at least three times, and the type A uncertainty (μ_A) was calculated by equation (6):

$$\mu_A = \sqrt{\frac{\sum_{i=1}^{n}(x_i - \bar{x})^2}{(n-1)\,n}} \quad (6)$$

where n is the experimental repetition time, x_i is the result of Experiment i and $\bar{x}$ is the average result of n experiments.

For the ICP–OES measurements, the analytical precision of the instrument (Agilent 730 spectrometer) was better than 3% relative standard deviation, and the type B uncertainty ($\mu_{B\text{-ICP}}$) was calculated by equation (7):

$$\mu_{B\text{-ICP}} = \frac{3\%\bar{x}}{\sqrt{3}} \quad (7)$$

For the pH measurements, the analytical precision of the instrument (FE28-Standard) was ±0.01, and the type B uncertainty (μ_B) was calculated to be $\mu_{B\text{-pH}} = \frac{0.01}{\sqrt{3}}$.

Finally, the combined standard uncertainty (μ) was calculated by equation (8):

$$\mu = \sqrt{\mu_A + \mu_B} \quad (8)$$

Characterization methods

Powder X-ray diffraction patterns were collected by using a Bruker D8 Advance diffractometer (copper source, 40 kV and 40 mA) over an angular range of 3–80° 2θ at a step size of 0.01° and a scan speed of 5° min^{-1}. Micro X-ray diffraction patterns were measured using a Rigaku D/Max Rapid diffractometer. Powder samples were inserted into a capillary tube with a diameter of 0.3 mm, sealed with Vaseline and then fixed on a rotary stage for measurement. The micro X-ray diffraction patterns were collected using a copper source (40 kV and 30 mA) equipped with a 0.1 mm collimator over a fixed omega angle (21°) and an oscillation phi angle (−115° ↔ −15°) at a speed of 1° per second with an exposure time of 100 seconds. The scanning electron microscopy images and energy-dispersive X-ray spectroscopy data were obtained by using a Hitachi SU8010 microscope after coating the samples with gold to increase their electrical conductivity. The transmission electron microscopy images were obtained by using an FEI Talos F200S microscope. XPS spectra were collected using a Thermo K-alpha spectrometer with an aluminium (Kα) source, of which the photon energy (hν) is 1,486.6 eV. The binding energies were corrected by using C 1s of 284.8 eV as a reference. The residual water-soluble N content of the soil was measured by using a UV–visible spectrophotometer (759S, Shanghai Lengguang Technology Co.). One gram of the solid sample was washed with 10 ml of deionized water, and the supernatant was separated from the soil by centrifugation and measured by a UV–visible spectrophotometer.

Reporting summary

Further information on research design is available in the Nature Research Reporting Summary linked to this article.

Data availability

All data generated for this study are available in the paper and the Supplementary Information.

References

1. Cockell, C. S. et al. Space station biomining experiment demonstrates rare earth element extraction in microgravity and Mars gravity. *Nat. Commun.* **11**, 5523 (2020).
2. Li, L. et al. General synthesis of 2D rare-earth oxide single crystals with tailorable facets. *Natl Sci. Rev.* **9**, nwab153 (2021).
3. Lee, J. C. K. & Wen, Z. Pathways for greening the supply of rare earth elements in China. *Nat. Sustain.* **1**, 598–605 (2018).
4. Xu, C. et al. Origin of heavy rare earth mineralization in South China. *Nat. Commun.* **8**, 14598 (2017).
5. Li, M. Y. H., Zhou, M.-F. & Williams-Jones, A. E. The genesis of regolith-hosted heavy rare earth element deposits: insights from the world-class Zudong deposit in Jiangxi province, South China. *Econ. Geol.* **114**, 541–568 (2019).
6. Stone, R. As China's rare earth R&D becomes ever more rarefied, others tremble. *Science* **325**, 1336–1337 (2009).
7. Zhou, F. et al. Selective leaching of rare earth elements from ion-adsorption rare earth tailings: a synergy between CeO_2 reduction and Fe/Mn stabilization. *Environ. Sci. Technol.* **55**, 11328–11337 (2021).
8. Li, M. Y. H., Zhou, M.-F. & Williams-Jones, A. E. Controls on the dynamics of rare earth elements during subtropical hillslope processes and formation of regolith-hosted deposits. *Econ. Geol.* **115**, 1097–1118 (2020).
9. Yang, X. J. et al. China's ion-adsorption rare earth resources, mining consequences and preservation. *Environ. Dev.* **8**, 131–136 (2013).
10. Balaram, V. Rare earth elements: a review of applications, occurrence, exploration, analysis, recycling, and environmental impact. *Geosci. Front.* **10**, 1285–1303 (2019).
11. Liu, W. S. et al. Water, sediment and agricultural soil contamination from an ion-adsorption rare earth mining area. *Chemosphere* **216**, 75–83 (2019).
12. Wang, Y. et al. Environmental risk assessment of the potential "chemical time bomb" of ion-adsorption type rare earth elements in urban areas. *Sci. Total Environ.* **822**, 153305 (2022).
13. Borst, A. M. et al. Adsorption of rare earth elements in regolith-hosted clay deposits. *Nat. Commun.* **11**, 4386 (2020).
14. Bao, Z. & Zhao, Z. Geochemistry of mineralization with exchangeable REY in the weathering crusts of granitic rocks in South China. *Ore Geol. Rev.* **33**, 519–535 (2008).
15. Li, M. Y. H. & Zhou, M.-F. The role of clay minerals in formation of the regolith-hosted heavy rare earth element deposits. *Am. Mineral.* **105**, 92–108 (2020).
16. Nie, W. et al. Research progress on leaching technology and theory of weathered crust elution-deposited rare earth ore. *Hydrometallurgy* **193**, 105295 (2020).
17. Lee, J. C. K. & Wen, Z. Rare earths from mines to metals: comparing environmental impacts from China's main production pathways. *J. Ind. Ecol.* **21**, 1277–1290 (2017).
18. Huang, X. W., Long, Z. Q., Wang, L. S. & Feng, Z. Y. Technology development for rare earth cleaner hydrometallurgy in China. *Rare Met.* **34**, 215–222 (2015).
19. *Cost of Pollution in China* (World Bank, 2007).
20. Li, J. et al. Study on aluminum removal through 5-sulfosalicylic acid targeting complexing and D290 resin adsorption. *Miner. Eng.* **147**, 106175 (2020).

21. He, Z., Zhang, Z., Yu, J., Xu, Z. & Chi, R. Process optimization of rare earth and aluminum leaching from weathered crust elution-deposited rare earth ore with compound ammonium salts. *J. Rare Earths* **34**, 413–419 (2016).
22. Judge, W. D. & Azimi, G. Recent progress in impurity removal during rare earth element processing: a review. *Hydrometallurgy* **196**, 105435 (2020).
23. Wang, Y. et al. Removal of aluminum from rare-earth leaching solutions via a complexation–precipitation process. *Hydrometallurgy* **191**, 105220 (2020).
24. Acar, Y. B. & Alshawabkeh, A. N. Principles of electrokinetic remediation. *Environ. Sci. Technol.* **27**, 2638–2647 (1993).
25. Acar, Y. B. et al. Electrokinetic remediation: basics and technology status. *J. Hazard. Mater.* **40**, 117–137 (1995).
26. Xu, J. et al. Remediation of heavy metal contaminated soil by asymmetrical alternating current electrochemistry. *Nat. Commun.* **10**, 2440 (2019).
27. Wang, Y. et al. Application of polypyrrole flexible electrode for electrokinetic remediation of Cr(VI)-contaminated soil in a main-auxiliary electrode system. *Chem. Eng. J.* **373**, 131–139 (2019).
28. Jones, C. J. F. P., Lamont-Black, J. & Glendinning, S. Electrokinetic geosynthetics in hydraulic applications. *Geotext. Geomembr.* **29**, 381–390 (2011).
29. Glendinning, S., Lamont-Black, J. & Jones, C. J. F. P. Treatment of sewage sludge using electrokinetic geosynthetics. *J. Hazard. Mater.* **139**, 491–499 (2007).
30. Martens, E. et al. Feasibility of electrokinetic in situ leaching of gold. *Hydrometallurgy* **175**, 70–78 (2018).
31. Martens, E. et al. Toward a more sustainable mining future with electrokinetic in situ leaching. *Sci. Adv.* **7**, eabf9971 (2021).
32. Wang, Y., Li, A. & Cui, C. Remediation of heavy metal-contaminated soils by electrokinetic technology: mechanisms and applicability. *Chemosphere* **265**, 129071 (2020).
33. Wen, D., Fu, R. & Li, Q. Removal of inorganic contaminants in soil by electrokinetic remediation technologies: a review. *J. Hazard. Mater.* **401**, 123345 (2021).
34. Li, X., Yang, Z., He, X. & Liu, Y. Optimization analysis and mechanism exploration on the removal of cadmium from contaminated soil by electrokinetic remediation. *Sep. Purif. Technol.* **250**, 117180 (2020).
35. Chen, Y. et al. Selective recovery of precious metals through photocatalysis. *Nat. Sustain.* **4**, 618–626 (2021).
36. Yang, L. et al. Bioinspired hierarchical porous membrane for efficient uranium extraction from seawater. *Nat. Sustain.* **5**, 71–80 (2022).
37. Alshawabkeh, A. N. & Acar, Y. B. Electrokinetic remediation. II: theoretical model. *J. Geotech. Eng.* **122**, 186–196 (1996).
38. He, Z. et al. Kinetics of column leaching of rare earth and aluminum from weathered crust elution-deposited rare earth ore with ammonium salt solutions. *Hydrometallurgy* **163**, 33–39 (2016).
39. Luo, X. et al. Removing aluminum from a low-concentration lixivium of weathered crust elution-deposited rare earth ore with neutralizing hydrolysis. *Rare Met.* **36**, 685–690 (2015).
40. Zhuang, Y. Large scale soft ground consolidation using electrokinetic geosynthetics. *Geotext. Geomembr.* **49**, 757–770 (2021).
41. Sun, T. R. & Ottosen, L. M. Effects of pulse current on energy consumption and removal of heavy metals during electrodialytic soil remediation. *Electrochim. Acta* **86**, 28–35 (2012).
42. Sun, T. R., Ottosen, L. M., Jensen, P. E. & Kirkelund, G. M. Effect of pulse current on acidification and removal of Cu, Cd, and As during suspended electrodialytic soil remediation. *Electrochim. Acta* **107**, 187–193 (2013).
43. Esrig, M. I. Pore pressures, consolidation, and electrokinetics. *J. Soil Mech. Found. Div.* **94**, 899–921 (1968).
44. Maidel, M. et al. Lanthanum recycling from spent FCC catalyst through leaching assisted by electrokinetic remediation: influence of the process conditions on mass transfer. *Sep. Purif. Technol.* **281**, 119905 (2022).
45. Xiao, Y. et al. Recovery of rare earths from weathered crust elution-deposited rare earth ore without ammonia-nitrogen pollution: I. Leaching with magnesium sulfate. *Hydrometallurgy* **153**, 58–65 (2015).
46. Xiao, Y. et al. Recovery of rare earth from the ion-adsorption type rare earths ore: II. Compound leaching. *Hydrometallurgy* **163**, 83–90 (2016).
47. Feng, J. et al. Effect of a novel compound on leaching process of weathered crust elution-deposited rare earth ore. *Miner. Eng.* **129**, 63–70 (2018).
48. Maes, S., Zhuang, W. Q., Rabaey, K., Alvarez-Cohen, L. & Hennebel, T. Concomitant leaching and electrochemical extraction of rare earth elements from monazite. *Environ. Sci. Technol.* **51**, 1654–1661 (2017).
49. Pires, C. M. G., Ponte, H. D. A., Pereira, J. T. & Ponte, M. J. J. D. S. Yttrium extraction from soils by electric field assisted mining applying the evolutionary operation technique. *J. Clean. Prod.* **227**, 272–279 (2019).
50. Zhuang, Y., Huang, Y., Liu, F., Zou, W. & Li, Z. Case study on hydraulic reclaimed sludge consolidation using electrokinetic geosynthetics. In *10th International Conference on Geosynthetics, Berlin, Germany (CD-ROM)* (German Geotechnical Society, 2014).
51. Xiao, Y. et al. Leaching and mass transfer characteristics of elements from ion-adsorption type rare earth ore. *Rare Met.* **34**, 357–365 (2015).

Acknowledgements

We thank J. Liu, Y. Zhu and Y. Xu in our group for their support in the field EKM experiments, discussions and suggestions. This work was supported by the Guangdong Major Project of Basic and Applied Basic Research (grant no. 2019B030302013 to H.H.), the National Key R&D Program of China (grant no. 2021YFC2901701 to H.H.), the National Natural Science Foundation of China (grant nos 41825003 to J.Z. and 42102037 to G.W.), the Guangdong Basic and Applied Basic Research Foundation (grant no. 2019A1515110720 to G.W.), the Guangdong Special Support Program (grant nos 2017TX04Z243 to R.Z. and 2019TX05L169 to J.Z.) and Science and Technology Planning of Guangdong Province, China (grant nos 2017B030314175 and 2020B1212060055). This is contribution no. IS-3245 from GIGCAS.

Author contributions

H.H. and J.Z. led the projects and designed the experiments. G.W. performed the experiments with assistance from J.X., L.R., S.K. and Y.W. H.H., G.W., J.Z., R.Z., X.L., J.W., L.M. and Y.Z. analysed the data. H.H., G.W., R.Z. and B.L. wrote the manuscript, which was revised by all authors.

Competing interests

The authors declare no competing interests.

Additional information

Supplementary information The online version contains supplementary material available at https://doi.org/10.1038/s41893-022-00989-3.

Correspondence and requests for materials should be addressed to Hongping He.

Peer review information *Nature Sustainability* thanks Zongguo Wen and the other, anonymous, reviewer(s) for their contribution to the peer review of this work.

Reprints and permissions information is available at www.nature.com/reprints.

Publisher's note Springer Nature remains neutral with regard to jurisdictional claims in published maps and institutional affiliations.

Springer Nature or its licensor (e.g. a society or other partner) holds exclusive rights to this article under a publishing agreement with the author(s) or other rightsholder(s); author self-archiving of the accepted manuscript version of this article is solely governed by the terms of such publishing agreement and applicable law.

© The Author(s), under exclusive licence to Springer Nature Limited 2022

nature research

Corresponding author(s): Hongping He

Last updated by author(s): Sep 14, 2022

Reporting Summary

Nature Research wishes to improve the reproducibility of the work that we publish. This form provides structure for consistency and transparency in reporting. For further information on Nature Research policies, see our Editorial Policies and the Editorial Policy Checklist.

Statistics

For all statistical analyses, confirm that the following items are present in the figure legend, table legend, main text, or Methods section.

n/a	Confirmed	
☒	☐	The exact sample size (*n*) for each experimental group/condition, given as a discrete number and unit of measurement
☒	☐	A statement on whether measurements were taken from distinct samples or whether the same sample was measured repeatedly
☒	☐	The statistical test(s) used AND whether they are one- or two-sided *Only common tests should be described solely by name; describe more complex techniques in the Methods section.*
☒	☐	A description of all covariates tested
☒	☐	A description of any assumptions or corrections, such as tests of normality and adjustment for multiple comparisons
☒	☐	A full description of the statistical parameters including central tendency (e.g. means) or other basic estimates (e.g. regression coefficient) AND variation (e.g. standard deviation) or associated estimates of uncertainty (e.g. confidence intervals)
☒	☐	For null hypothesis testing, the test statistic (e.g. *F*, *t*, *r*) with confidence intervals, effect sizes, degrees of freedom and *P* value noted *Give P values as exact values whenever suitable.*
☒	☐	For Bayesian analysis, information on the choice of priors and Markov chain Monte Carlo settings
☒	☐	For hierarchical and complex designs, identification of the appropriate level for tests and full reporting of outcomes
☒	☐	Estimates of effect sizes (e.g. Cohen's *d*, Pearson's *r*), indicating how they were calculated

Our web collection on statistics for biologists contains articles on many of the points above.

Software and code

Policy information about availability of computer code

Data collection	No software was used for data collection. All data were collected from experiments.
Data analysis	XPS was analysed with Thermo Avantage software (V5.934)

For manuscripts utilizing custom algorithms or software that are central to the research but not yet described in published literature, software must be made available to editors and reviewers. We strongly encourage code deposition in a community repository (e.g. GitHub). See the Nature Research guidelines for submitting code & software for further information.

Data

Policy information about availability of data

All manuscripts must include a data availability statement. This statement should provide the following information, where applicable:

- Accession codes, unique identifiers, or web links for publicly available datasets
- A list of figures that have associated raw data
- A description of any restrictions on data availability

Data availability: All data generated for this study are available within the paper and Supplementary Information.

Field-specific reporting

Please select the one below that is the best fit for your research. If you are not sure, read the appropriate sections before making your selection.

☐ Life sciences ☐ Behavioural & social sciences ☒ Ecological, evolutionary & environmental sciences

For a reference copy of the document with all sections, see nature.com/documents/nr-reporting-summary-flat.pdf

Ecological, evolutionary & environmental sciences study design

All studies must disclose on these points even when the disclosure is negative.

Study description	Electrokinetic mining experiments in three scales: bench-scale, scale-up, and field scales.
Research sample	Research sample: a weathering crust in Guangzhou, South China. Sample choice reason: more than 95% of heavy rare earth elements is mined from ion-adsorption rare earth deposits of weathering crusts in South China.
Sampling strategy	No statistical method was used to predetermine sample size.
Data collection	The leachate was collected at different time intervals during the electrokinetic treatment time and analyzed by the inductively coupled plasma optical emission spectrometry (ICP-OES) by G.W. The pH of the leachate was monitored with a pH meter by G.W. Characterizations including XRD, SEM, EDS, TEM, and XPS were performed by G.W. with assistance from J.X., L.R., S.K., and Y.W.
Timing and spatial scale	The data of the field experiment were collected from 11/08/2021 to 22/08/2021 in each 12 h. The experiment was carried out for 11 days, and we can collect enough data in this way. In each time interval, 24 samples were taken from different spatial locations in order to describe the REE variations in 3D scale. Around 100 g of sample was taken from the experimental ore each time, which is enough for analysis but negligible for the 14 tons scale experimental ore.
Data exclusions	no data were excluded from the analyses
Reproducibility	A total of 24 samples were collected each time in field experiment, confirming the accuracy and reproducibility. Bench-scale and scale-up experiments were carried out in triplicate . All attempts to repeat the experiment were successful
Randomization	No sample allocation was involved in this study
Blinding	No blinding was involved in this study, because this study focuses on engineering problems of the newly proposed technology.

Did the study involve field work? ☒ Yes ☐ No

Field work, collection and transport

Field conditions	The climate of Guangzhou is subtropical monsoon climate. The average temperature is 32 °C without raining during experiment.
Location	The location of Guangzhou is at 112°57′ - 114°3′E longitude and 22°26′ - 23°56′N latitude.
Access & import/export	It is not involved in this study.
Disturbance	There is no disturbance.

Reporting for specific materials, systems and methods

We require information from authors about some types of materials, experimental systems and methods used in many studies. Here, indicate whether each material, system or method listed is relevant to your study. If you are not sure if a list item applies to your research, read the appropriate section before selecting a response.

Materials & experimental systems

n/a	Involved in the study
☒	☐ Antibodies
☒	☐ Eukaryotic cell lines
☒	☐ Palaeontology and archaeology
☒	☐ Animals and other organisms
☒	☐ Human research participants
☒	☐ Clinical data
☒	☐ Dual use research of concern

Methods

n/a	Involved in the study
☒	☐ ChIP-seq
☒	☐ Flow cytometry
☒	☐ MRI-based neuroimaging